High-Gain and Narrow-Bandwidth Optical Amplifier via Optomechanical Four-Wave Mixing

Zongyang Li,[1,2] Zhenqiang Ren,[1,2] Yongmin Li,[1,2,*] Yong-chun Liu,[3,†] and Kunchi Peng[1,2]

[1] *State Key Laboratory of Quantum Optics and Quantum Optics Devices, Institute of Opto-Electronics, Shanxi University, Taiyuan 030006, P. R. China*

[2] *Collaborative Innovation Center of Extreme Optics, Shanxi University, Taiyuan, Shanxi 030006, P. R. China*

[3] *State Key Laboratory of Low-Dimensional Quantum Physics and Department of Physics, Tsinghua University, Collaborative Innovation Center of Quantum Matter, Beijing 100084, P. R. China*

(Received 24 August 2018; revised manuscript received 31 March 2019; published 20 June 2019)

We present an ultrahigh gain, narrow bandwidth, and low noise optical amplifier via the radiation pressure induced by the four-wave mixing (FWM) effect based on a cavity optomechanical system in the unresolved sideband regime. It offers a favorable platform to amplify a weak signal field and simultaneously generate a conjugate field with tunable gain and bandwidth. We achieve an ultranarrow bandwidth (9 Hz) and ultrahigh gain (40 dB) optical field amplification at a weak pump power (10 μW). Due to the unresolved sideband regime, the system supports simultaneous multimode amplification. The presented optomechanical FWM mechanism-based amplifier can provide standard quantum-noise-limit amplification, in principle, and is applicable to a broad range of the electromagnetic spectrum ranging from the microwave band to the ultraviolet band.

DOI: 10.1103/PhysRevApplied.11.064048

I. INTRODUCTION

A narrow-band, high-gain, and low-noise optical amplifier can provide remarkable coherent amplification for a weak narrow-band signal field, while keeping the out-of-band noise intact. When combined with a narrow-band filter [1] or a neutral optical attenuator, an optical filter with gain can be realized. It plays a key role in weak signal detection in optical communication, lidar remote sensing systems [2], and so on. The gravitational wave detector in space [3,4] can detect gravitational wave signals in low-frequency bands less than 1 Hz. However, the collected optical signal from remote satellites has a typical value of only several picowatts even if more than one watt of laser beam has been launched millions of kilometers away. The local laser at the receiver must be phase locked to the weak incoming beam by using heterodyne phase locking [5]. In this scenario, a narrow-band (on the hertz level), high-gain, and low-noise optical amplifier is helpful to improve the phase locking.

As a typical nonlinear optical phenomenon, four-wave mixing (FWM) has been observed in various media including nonlinear crystals, atomic vapors [6,7], optical fibers [8], grapheme [9], and organic polymers [10], and has found crucial applications in the fields of optical communication [11], sensing [12], imaging [13], quantum information [7], and so on. Cavity optomechanical systems [14], which combine mechanical resonators, electromagnetic fields, and optical cavities, have found various applications such as gravitational wave detection [15], optomechanical induced transparency (OMIT) and amplification [16–23], squeezing or entanglement of light fields and mechanical oscillators [24–29], and interfaces between microwave and optical light [30]. In order to form a double Λ energy level, which is indispensable for the FWM process, mechanical mode splitting either in the strong optomechanical coupling regime [31] or by additional coherent mechanical driving [32,33] are investigated in the resolved side-band regime. Although optical amplification via optomechanical interaction was observed in resolved side-band systems [19,20] due to the heating effect of a blue detuned pump field, the systems cannot remain stable for a large pump power and provide adequate optical gain.

Here, we report an implementation of an optical amplifier via the FWM process induced by radiation pressure in an unresolved side-band optomechanical system, where the dissipation of the optical cavity is well beyond the resonance frequency of the mechanical resonator. An ultrahigh gain, narrow-bandwidth and low-noise optical amplification for a picowatt level input optical field is observed at the microwatt level pump power. Due to the large linewidth of the optical cavity, which covers multiple mechanical modes, the radiation pressure coupling

*liyongminwj@163.com
†ycliu@tsinghua.edu.cn

between the cavity fields and mechanical modes results in the formation of a series of double Λ configuration energy levels, which enable the observation of multimode FWM phenomena [34]. Due to its narrow-bandwidth frequency response characteristics, the presented amplifier may find potential applications in optical or microwave frequency standards [35] and gravitational wave detectors in space. On the other hand, the present work paves the way for integrated microscale optical narrow-band amplification devices with low pump energy.

II. OPTOMECHNICAL FWM

The FWM mechanism exploits a double Λ level scheme in an unresolved side-band cavity optomechanical system [Fig. 1(a)]. In the figure, n_c and m denote the photon and phonon occupation numbers of the cavity and mechanical modes, respectively. A strong red-detuned pump field a_p (frequency ω_p) with detuning $\Delta_{\rm eff}$ from the cavity resonance frequency couples the energy transition $|n_c, m\rangle \leftrightarrow |n_c+1, m\rangle$ and $|n_c, m+1\rangle \leftrightarrow |n_c+1, m+1\rangle$. A weak signal field a_s (frequency ω_s), which is blue detuned to the pump laser with detuning $\Delta_s \approx \omega_m$, couples the transition $|n_c, m\rangle \leftrightarrow |n_c+1, m+1\rangle$, where ω_m is the mechanical resonance frequency. Based on this level configuration, the input signal field can be amplified remarkably and the associated FWM field a_F (frequency ω_F) is generated simultaneously. The frequencies involved in this FWM parametric process follow the law of energy conservation $2\omega_p = \omega_s + \omega_F$.

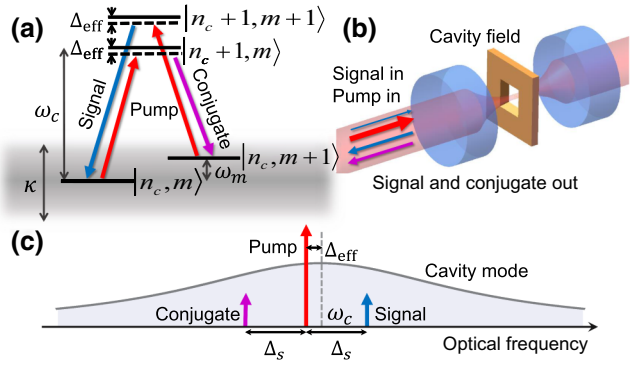

FIG. 1. FWM in an unresolved side-band optomechanical system. (a) Level scheme of the optomechanical system in the unresolved side-band regime. (b) Sketch of the FWM experiment in a MIM system. The signal and pump fields with appropriate detuning are injected into the optomechanical system, then the optomechanical interaction amplifies the signal field and simultaneously generates the conjugate field. (c) Schematic diagram of the various optical fields. The pump field is red detuned to the cavity resonance to control the mechanical motion. The signal is blue detuned to the pump laser with detuning frequency Δ_s. The generated FWM and signal fields are situated symmetrically along the two sides of the pump field.

In the optomechanical FWM process, the beating of the signal and pump fields inside the optical cavity generates a periodic radiation pressure force [Fig. 1(b)], which dynamically drives the mechanical motion with beating frequency $\Delta_s = \omega_s - \omega_p$. The frequency of the intracavity pump field is modulated in turn by the driven mechanical motion with $\delta\omega_p(t) = G\delta x(t)$, which generates the Stokes and anti-Stokes side-band fields with a frequency of $\omega_p \pm \Delta_s$, where $G = \partial\omega_p/\partial x$ is the optical frequency shift per unit displacement of the mechanical resonator. In this scenario, the signal field is amplified due to the excitation of the Stokes field with exactly the same frequency, accompanied by the conjugate field (anti-Stokes side-band). The frequency response of the FWM process depends on the susceptibility of the optical cavity and the effective mechanical susceptibility of the mechanical resonator, which, in turn, relies on the optical spring effect and optomechanical damping caused by the detuned pump field.

In the case of a strong pump field, the operator of the mechanical and cavity mode can be written as its steady-state value plus an additional operator with zero mean value $b = \beta + \delta b$ and $a = (\alpha + d)e^{-i\omega_p t}$. The initial detuning of the pump field is slightly shifted to $\Delta_s = \omega_p - (\omega_c + G\bar{x})$ by the static-radiation-pressure-induced displacement of the resonator originating from the intracavity mean field α, where ω_c is the bare cavity resonance frequency. The power transmission of this FWM process, which is defined as the ratio of the amplified signal and conjugate field power returned from the system divided by the input signal power, is given by (Appendix B)

$$\begin{aligned} M_s(\Delta_s) &= |\kappa_{\rm ex}\chi_c(\Delta_s)[1 + 2i\omega_m|g|^2 \\ &\quad \times X_{\rm eff}(\Delta_s)\chi_c(\Delta_s)] - 1|^2, \\ M_F(-\Delta_s) &= 4\omega_m^2\kappa_{\rm ex}^2|g|^4|\chi_c^2(-\Delta_s)X_{\rm eff}(\Delta_s)|^2, \end{aligned} \quad (1)$$

where $X_{\rm eff}^{-1}(\omega) = \chi_m^{*-1}(-\omega)\chi_m^{-1}(\omega) - 2ig^2\omega_m[\chi_c(\omega) - \chi_c^*(-\omega)]$ is the effective mechanical susceptibility in the presence of the optomechanical interaction, $g = g_0\alpha$ is the light-enhanced optomechanical coupling strength, and $\chi_c(\omega) = (-i\Delta_{\rm eff} - i\omega + \kappa/2)^{-1}$ and $\chi_m(\omega) = (i\omega_m - i\omega + \Gamma_m/2)^{-1}$ are the optical and mechanical susceptibilities of the optical cavity and mechanical resonator, respectively. The optomechanical interaction of the system produces a double-gain window for the signal field around $\Delta_s \approx \pm\omega_m$. The frequency response of the FWM process is approximately equal to the effective mechanical susceptibility $X_{\rm eff}(\Delta_s)$ for a sufficiently large cavity linewidth κ.

III. EXPERIMENT AND RESULTS

In our experiment, we exploit a membrane-in-the-middle (MIM) system, more specifically, a Si_3N_4 high-tension membrane inside a Fabry-Perot cavity serves

as the cavity optomechanical system [20,24,36–38]. The resonance frequencies of its (1, 1) and (2, 2) modes are 585 and 1170 kHz, respectively. The quality factor is 0.61×10^6 for the (1, 1) mode and 1.36×10^6 for the (2, 2) mode at room temperature. The optical cavity consists of a concave mirror with high reflectivity and a flat mirror with relatively low reflectivity, which serves as the input coupler. The cavity operates in an overcoupling regime with linewidth $\kappa/2\pi = 3.5$ MHz and escape efficiency $\kappa_{ex}/\kappa = 0.91$. The single-photon optomechanical coupling strength is determined to be $g_0/2\pi = 13$ Hz. The above experimental parameters place the system well into the unresolved side-band regime.

The schematic of our experimental setup is shown in Fig. 2(a). A 1064-nm laser is divided into three parts by two fiber couplers (FC1 and FC2). Among them, two parts are frequency-shifted by 150 MHz (pump field) and $150 + \Delta_s/2\pi$ MHz (signal field) using two fiber acoustic optical modulators (AOM1 and AOM2) [Fig. 2(b)], and then combined together at another fiber coupler (FC3). Since the frequency differences among the amplified signal, conjugate field, and pump field are at a level less than MHz, they can hardly be separated by a common optical method. To individually measure the amplified signal and conjugate field, the reflected field of the system is monitored via a heterodyne detection device. In order to eliminate the effect of the radio frequency modulation signals on the spectrum measurement, the third part of the laser is shifted by 80 MHz by an acoustic optical modulator in free space (AOM3) to serve as the local oscillator (LO) of the heterodyne system.

The pump laser is frequency locked to the optical cavity with detuning Δ_{eff}, which is achieved by adding a dc bias on the error signal of the servo system. An optical Faraday rotator (OFR) is used to extract the reflective field of the MIM system. The majority of the reflected field is detected by a heterodyne system and the resulting beating photocurrent signal between the LO and reflected field is successively monitored by a spectrum analyzer. The remaining reflective field is used for cavity length locking (not shown in the sketch). By sweeping the radio frequency signal applied on the AOM in the signal field, the peak values of the beat signal spectrum proportional to the amplified signal (conjugate) field power are continuously recorded using the spectrum analyzer.

Figure 3 shows the normalized frequency response of the amplified signal and FWM fields, corresponding to the power gain defined in Eq. (1). The FWM process is observed clearly with power gains over 30 dB and a bandwidth of about 100 Hz despite a pump power of only 15 μW (the power of the original signal is 1.08 pW). The optomechanical system in the unresolved side-band regime could support the interaction between one optical mode and multiple mechanical modes, which enables the multimode FWM phenomenon. Figure 3(b) shows the experimental observation of such a phenomenon induced by a higher-order mechanical mode, giving clear evidence of the multimode radiation-pressure-induced FWM process in our unresolved side-band optomechanical system.

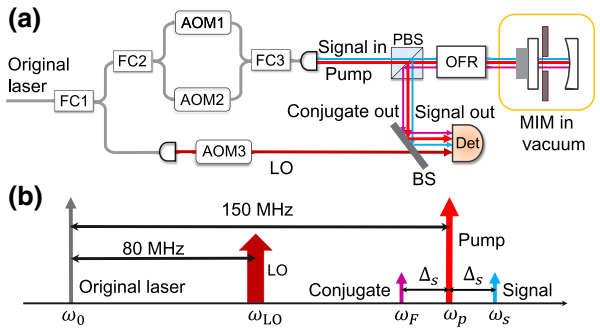

FIG. 2. Optical amplifier via FWM process in a MIM optomechanical system. (a) Sketch of the optomechanical FWM experiment. The MIM system is located in a vacuum cavity where a vibration isolator is used to suppress the environmental vibration noise. AOM1 and AOM2 are fiber-coupled acoustic optical modulators while AOM3 is an acoustic optical modulator in free space. (b) Schematic diagram of the various optical frequencies involved in the FWM experiment. Det, heterodyne detector; OFR, optical Faraday rotator; LO, local oscillator; BS, beam splitter; PBS, polarizing beam splitter.

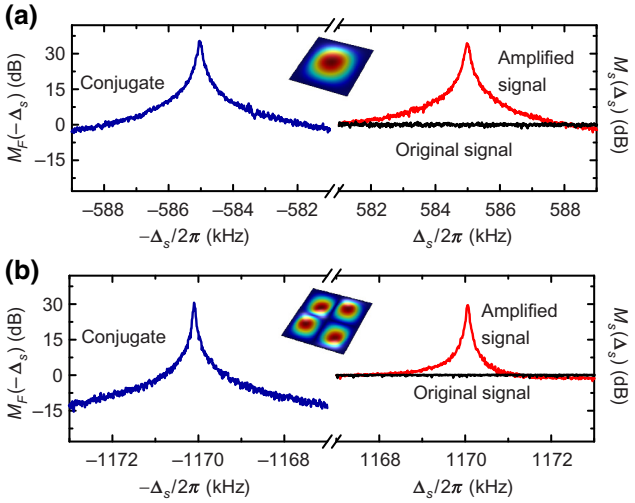

FIG. 3. Observation of the optical amplification via FWM process. The amplified signal and generated conjugate field are represented by red and blue curves in the diagram, respectively. The black curve shows the original signal intensity measured by setting the signal field far off resonance to the cavity resonance. (a) The (1, 1) mode of the membrane resonator with resonance frequency of 585 kHz is involved in the optomechanical interaction. (b) The optical amplification and FWM process arising from the (2, 2) mode with resonance frequency of 1170 kHz.

The frequency response of the power transmissions is subject to the mechanical motion when the optical driving is nearly resonant with the mechanical motion. On the other hand, when the optical driving is far off resonance to the mechanical motion, the FWM process is very weak with a power transmission of the signal field slightly lower than 1 due to the imperfect reflection of the over-coupling optical cavity.

For a sufficient large cavity linewidth, the frequency response of the FWM process closely depends on the effective mechanical susceptibility of the mechanical resonator, which can be formulated by the effective mechanical damping rate $\Gamma_{\rm eff}$ and resonance frequency $\omega_{\rm eff}$ of the mechanical motion as $X_{\rm eff}^{-1} = \omega_{\rm eff}^2 - \omega^2 - i\omega\Gamma_{\rm eff}$. Therefore, we can manipulate the FWM process via controlling the mechanical motion. The maximum gain in the bad cavity limit $\kappa \gg \omega_m$ is achieved when the optical driving is resonant to the mechanical motion $|\Delta_s| = \omega_{\rm eff}$ (Appendix C)

$$M_{\rm max} = \frac{64|g|^4\kappa_{\rm ex}^2}{\kappa^4\Gamma_{\rm eff}^2}. \tag{2}$$

For a high Q mechanical resonator, the effective mechanical damping rate is dominated by the optomechanical damping $\Gamma_{\rm eff} \approx \Gamma_{\rm opt}$. In this case, the bandwidth of the amplifier is dependent on the optomechanical damping rate in the bad cavity limit

$$\Gamma_{\rm opt} = -g_0^2 n_c \frac{4\Delta_{\rm eff}\kappa\omega_m}{(\kappa^2/4 + \Delta_{\rm eff}^2)^2}. \tag{3}$$

According to Eqs. (2) and (3), the gain and window width of the optical amplifier depend on the optomechanical coupling strength g and the optomechanical damping rate $\Gamma_{\rm opt}$, which are tunable by the intensity and detuning of the pump field.

By experimentally shifting the effective detuning $\Delta_{\rm eff}/2\pi$ from 60 to 620 kHz while keeping the pump intensity constant at 15 μW, the gain coefficients are significantly suppressed, accompanied by a broadening of the bandwidth due to the increased optomechanical damping rate [Fig. 4(a)]. The effect of varying the pump power is shown in Fig. 4(b), where we set the detuning of the pump field $\Delta_{\rm eff}/2\pi = 270$ kHz and vary the pump intensity from 5 to 20 μW. The above experimental observations agree well with the theoretical predictions (Appendix C) and indicate that the gain and bandwidth of the optical amplifier can be manipulated by controlling the detuning and power of the pump field. Thus, the presented optomechanical system offers a favorable platform to achieve the optical amplification with a tunable window width, which is difficult to achieve in other systems. Moreover, the system can serve as a high-gain optical amplifier at a low pump power condition, and the intensity gain is nearly pump-power independent.

Optical systems with ultranarrow response bandwidth have potential applications in various fields such as optical frequency standards [35] and gravitational wave detection [15]. Figure 5 shows that the small detuning and low power of the pump field enable a large gain and narrow window width FWM. Given the same detuning of the pump field, the optomechanical damping rate is smaller for the higher-order mechanical modes due to their higher resonance frequencies. By using the (2, 2) mode of the mechanical resonator and setting the pump field detuning around 10 kHz, with a pump power of 10 μW an extremely high intensity gain of 40 dB and ultranarrow frequency response bandwidth of 9 Hz is achieved via the optomechanical amplifier (Fig. 5).

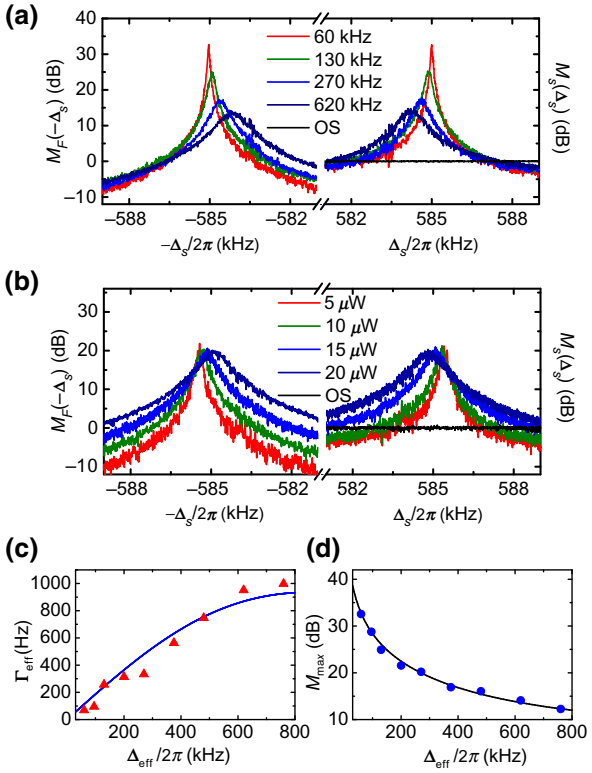

FIG. 4. Observed frequency response of the FWM. The maximum gain and window width are manipulated by varying the detuning of the pump field under a constant pump power (a) and varying the pump power while keeping a constant detuning (b). The black curve represents the normalized original signal (OS) intensity without FWM and the colored lines show the frequency response of the FWM process at different detuning values or intensities of the pump field. (c),(d), The variation of the window width and maximum gain as a function of the detuning of the pump field, where the red triangle and blue solid circles represent the measured values and the line represents the theoretical predictions.

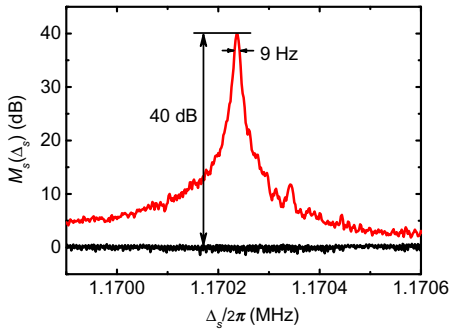

FIG. 5. High intensity gain, ultranarrow bandwidth optical amplification. Using a nearly resonant and low-power pump field combined with a (2, 2) mechanical mode, the optomechanical damping rate can be suppressed greatly. In this way, a 9-Hz bandwidth frequency response window with a 40-dB intensity gain has been achieved.

IV. THE ADDED NOISES

As an optical amplifier, the added noises should be taken into consideration. Two factors are responsible for such noises in our system: the intrinsic thermal motion of the mechanical resonator and the radiation-pressure shot noise of the pump field [39]. To derive the added noises, we omit the signal field while retaining the thermal driving and vacuum fluctuation terms of Eq. (A3)

$$\begin{aligned}\chi_c^{-1}(\omega)d(\omega) &= -ig[\delta b^\dagger(\omega)+\delta b(\omega)]+\sqrt{\kappa_{\rm ex}}d_v(\omega)\\ &\quad+\sqrt{\kappa_0}a_v(\omega),\\ \chi_m^{-1}(\omega)\delta b(\omega) &= -i[g^* d(\omega)+g d^\dagger(\omega)]+\sqrt{\Gamma_m}b_{\rm th}(\omega).\end{aligned} \tag{4}$$

Starting from Eq. (4), the reflective field from the cavity can be expressed as

$$\begin{aligned}d_r(\omega) &= 2i\omega_m\chi_c(\omega)X_{\rm eff}(\omega)\\ &\times\left\{\begin{array}{c}\kappa_{\rm ex}[|g|^2\chi_c(\omega)d_v(\omega)+g^2\chi_c^*(-\omega)d_v^\dagger(\omega)]\\ +\sqrt{\kappa_{\rm ex}\kappa_0}[|g|^2\chi_c(\omega)a_v(\omega)+g^2\chi_c^*(-\omega)a_v^\dagger(\omega)]\end{array}\right\}\\ &-ig\sqrt{\Gamma_m\kappa_{\rm ex}}\chi_c(\omega)X_{\rm eff}(\omega)[\chi_m^{*-1}(-\omega)b_{\rm th}(\omega)+\chi_m^{-1}(\omega)b_{\rm th}^\dagger(\omega)]\\ &+\chi_c(\omega)\left[\kappa_{\rm ex}d_v(\omega)+\sqrt{\kappa_{\rm ex}\kappa_0}a_v(\omega)\right]-d_v(\omega).\end{aligned} \tag{5}$$

Then, the spectrum of the added noise photon number takes the form

$$\begin{aligned}N_r(\omega) &= \langle d_r(\omega)^\dagger d_r(\omega)\rangle\\ &= 4\omega_m^2\kappa_{\rm ex}\kappa|g|^4|\chi_c^2(-\omega)X_{\rm eff}(\omega)|^2\\ &\quad+|g|^2\Gamma_m\kappa_{\rm ex}|\chi_c(\omega)X_{\rm eff}(\omega)|^2[|\chi_m^{-1}(-\omega)|^2 n_{\rm th}\\ &\quad+|\chi_m^{-1}(\omega)|^2(n_{\rm th}+1)].\end{aligned} \tag{6}$$

where $n_{\rm th}=k_BT/\hbar\omega_m$ denotes the average thermal phonon number of the mechanical mode at temperature T and k_B is the Boltzmann constant. The first term on the right-hand side of Eq. (6) represents the effect of the radiation-pressure shot noise of the pump field and the second term represents the effect of thermal motion of the mechanical resonator.

When referring the added noise to the input port of the amplifier, the resulting input noise power is defined as

$$P_N=\hbar\omega N_r(\omega)/M_s(\omega). \tag{7}$$

For the current setup operating at room temperature, the thermal motion is the dominant noise source in the amplification process. Since the mechanical resonator is driven by the modulated radiation pressure of the cavity field in the FWM process, even if the signal field is absent, the thermal motion of the resonator itself can also induce the FWM process and contribute to the added noise. In order to measure the added noise in the optomechanical amplifier, we block the signal beam and use the same experimental parameters as in Fig. 2(a). The measured noise is $P_N\approx 3$ fW/Hz at the peak gain point $\omega=\omega_{\rm eff}$. By using the experimental parameters and Eq. (7), the theoretical input noise power spectrum is calculated to be 0.62 fW/Hz. The discrepancy between the theoretical prediction and the experimental observations probably arises from other thermal vibration noises of the system including the chip substrate and cavity mirror, which are not included in our theoretical model, rather than the membrane itself.

Nevertheless, the added noise can be suppressed by setting the system at a cryogenic temperature. As simulated in Fig. 6, with a low temperature of $T=10$ mK, the added noise photons of the optomechanical amplifier can be less than 1.2 photons per hertz. For a lower temperature of $T=1$ mK, the added noise can reach the quantum noise limit of a phase-insensitive linear amplifier, that is, 1 photon per hertz. In this scenario, the radiation pressure shot noise of the pump field is the dominant noise source. When

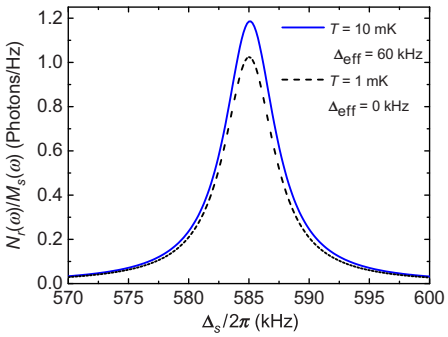

FIG. 6. Simulated noise photon spectrum $N_r(\omega)/M_s(\omega)$ of the optomechanical amplifier (referred to the input port of the amplifier) at different temperatures. Other parameters are the same as in Fig. 3.

the detuning of the signal frequency is far from the resonance frequency $\omega_{\rm eff}$ of the mechanical motion, the added noise tends to zero quickly, which means no excess noise is introduced. It is noted that the excess noise beyond the quantum noise limit depends on the average thermal phonon number of the mechanical mode $n_{\rm th}$ at a nonzero temperature. Therefore, for a mechanical resonator with a very high resonance frequency above gigahertz, the strict requirement of a cryogenic temperature is not necessary for a quantum noise limit operation due to the sufficiently low phonon population of the mechanical mode.

V. CONCLUSION

We propose and demonstrate a high-gain, low-noise, and narrow bandwidth optical amplifier via a radiation-pressure-induced FWM phenomenon in an unresolved side-band optomechanical system. The system requires only a microwatt-level pump power to achieve a remarkable intensity gain for a weak signal field at the picowatt level. The added noise of the optomechanical amplifier can reach the standard quantum noise limit of a phase-insensitive linear amplifier when operating in a cryogenic temperature or using a mechanical resonator with a high resonance frequency above gigahertz.

In comparison with other media that allow optical amplification, such as atomic systems and nonlinear crystals, cavity optomechanical systems with tunable energy levels, which depend on the parameters of the optical cavity and mechanical resonator, can be operated in a broad wavelength range, ranging from the microwave to ultraviolet bands. Meanwhile, as demonstrated in our experiment, the intensity gain and bandwidth of the amplifier can be dynamically tuned by optical driving, which is difficult to achieve in other media. By tuning the optomechanical damping through the pump field, the gain bandwidth of the optical amplifier can be as narrow as a few hertz or even below the hertz level. Such a device is well suited for the scenarios where detection of a weak narrow-band signal is required. Moreover, by suppressing the added noises induced by the mechanical thermal motion, our system may allow the generation of a quantum entanglement between the amplified and the conjugate modes [27–29].

ACKNOWLEDGMENTS

This work is supported by the National Key R&D Program of China (Grant No. 2016YFA0301403); National Natural Science Foundation of China (NSFC) (Grants No. 11774209, No. 61378010, No. 11674390, and No. 91736106); Shanxi 1331KSC; Key Research and Development Projects of Shanxi Province (Grant No. 201803D121065); China Postdoctoral Science Foundation (Grant No. 2018M642807).

APPENDIX A: THEORETICAL MODEL

The Hamiltonian of an optomechanical system in an unresolved side-band regime is given by

$$\begin{aligned} H &= H_{\rm free} + H_{\rm int} + H_{\rm drive}, \\ H_{\rm free} &= \omega_c a^\dagger a + \omega_m b^\dagger b, \\ H_{\rm int} &= g_0 a^\dagger a (b^\dagger + b), \\ H_{\rm drive} &= i\sqrt{\kappa_{\rm ex}}(\alpha_p e^{-i\omega_p t} a^\dagger + \alpha_s e^{-i\omega_s t} a^\dagger) + {\rm H.}c., \end{aligned} \tag{A1}$$

where $H_{\rm free}$, $H_{\rm int}$, and $H_{\rm drive}$ denote the free Hamiltonian, optomechanical interaction part of the Hamiltonian, and optical driving of the system, respectively. The operators a and b denote the annihilation operator of the cavity field with bare cavity resonance frequency ω_c, and the mechanical mode with resonance frequency ω_m, respectively. The operator b is related to the displacement operator via $x/x_{\rm ZPF} = b + b^\dagger$, where $x_{\rm ZPF} = \sqrt{\hbar/2m_{\rm eff}\omega_m}$ is the zero-point fluctuation and $m_{\rm eff}$ is the effective mass of the mechanical mode. The coefficient $g_0 = G x_{\rm ZPF}$ denotes the single-photon optomechanical coupling strength and $G = \partial\omega_c/\partial x$ is the optical frequency shift per unit displacement of the resonator. The value $\kappa_{\rm ex}$ represents the dissipation associated with the input coupling of the optical cavity and the total dissipation of the optical mode is $\kappa = \kappa_{\rm ex} + \kappa_0$. The driving fields consist of pump field ω_p with amplitude $\alpha_p = \sqrt{P_p/\hbar\omega_p}e^{-i\phi_p}$ and signal field ω_s with amplitude $\alpha_{\rm s} = \sqrt{P_{\rm s}/\hbar\omega_{\rm s}}e^{-i\phi_{\rm s}}$, where $P_p(P_s)$, $\phi_p(\phi_s)$ denote the input power and phase of the pump (signal) field. Hereafter, we assume $P_p \gg P_s$ to ensure an undepleted pump approximation.

In a frame rotating at the frequency of the pump field $a_0 = a e^{i\omega_p t}$, the nonlinear quantum Langevin equations of the system can be expressed as

$$\begin{aligned} \dot{a}_0 &= \left(i\Delta_0 - \frac{\kappa}{2}\right) a_0 - i g_0 a_0 (b^\dagger + b) + \sqrt{\kappa_{\rm ex}}(\alpha_p + \alpha_s e^{-i\Delta_s t}) \\ &\quad + \sqrt{\kappa_{\rm ex}} d_{\rm in} + \sqrt{\kappa_0} a_v, \\ \dot{b} &= -\left(\frac{\Gamma_m}{2} + i\omega_m\right) b - i g_0 a_0^\dagger a_0 + \sqrt{\Gamma_m} b_{\rm th}, \end{aligned} \tag{A2}$$

where $\Delta_0 = \omega_p - \omega_c$ and $(\Delta_s = \omega_s - \omega_p)$ denote the frequency difference between the pump field and the cavity mode (the signal and pump field). $\Gamma_m = \omega_m/Q_m$ is the dissipation of the mechanical mode, where Q_m is the mechanical quality factor, $d_{\rm in}$ denotes the fluctuations of the driving fields, a_v denotes the vacuum noise associated with the optical dissipation, and $b_{\rm th}$ represents the thermal drive to the resonator.

We express the optical and mechanical modes as the sum of the mean fields at the steady state and the fluctuation term: $a_0 = \alpha + d$, $b = \beta + \delta b$. From Eq. (A2), we can obtain the values of the mean field at the steady

state for the optical cavity mode and mechanical mode as $\alpha = 2\sqrt{\kappa_{ex}}\alpha_p/\kappa - i\Delta_{eff}$ and $\beta = g_0|\alpha|^2/\omega_m$. By neglecting the nonlinear terms, the linearized quantum Langevin equations of the fluctuations for the optical and mechanical modes d and δb are given by

$$\begin{aligned}\dot{d}(t) &= -\left(\frac{\kappa}{2} - i\Delta_{eff}\right)d(t) - ig_0\alpha[\delta b^\dagger(t) + \delta b(t)] \\ &\quad + \sqrt{\kappa_{ex}}\alpha_s e^{-i\Delta_s t} + \sqrt{\kappa_{ex}}d_{in} + \sqrt{\kappa_0}a_v, \\ \delta\dot{b}(t) &= -\left(\frac{\Gamma_m}{2} + i\omega_m\right)\delta b(t) - ig_0[\alpha^* d(t) + \alpha d^\dagger(t)] \\ &\quad + \sqrt{\Gamma_m}b_{th}.\end{aligned} \tag{A3}$$

Note that the detuning of the pump field is slightly shifted to $\Delta_{eff} = \Delta_0 + G\bar{x}$ due to the static-radiation-pressure-induced displacement $\bar{x} = x_{ZPF}(\beta^* + \beta)$ of the resonator originating from the intracavity mean field.

We neglect the thermal noise b_{th} and the small fluctuations of the optical fields d_{in} and a_v. In this case, we convert Eq. (A3) into the frequency domain using the Fourier transform

$$\begin{aligned}\chi_c^{-1}(\omega)d(\omega) &= -ig[\delta b^\dagger(\omega) + \delta b(\omega)] + \sqrt{\kappa_{ex}}a_s(\omega - \Delta_s), \\ \chi_m^{-1}(\omega)\delta b(\omega) &= -i[g^* d(\omega) + g d^\dagger(\omega)],\end{aligned} \tag{A4}$$

where $g = g_0\alpha$ is the light-enhanced optomechanical coupling strength, $\chi_c^{-1}(\omega) = -i\Delta_{eff} - i\omega + \kappa/2$ is the optical susceptibility of the cavity, and $\chi_m^{-1}(\omega) = i\omega_m - i\omega + \Gamma_m/2$ is the mechanical susceptibility. As the system is in the unresolved side-band regime, the mechanical response can be described by the effective mechanical susceptibility in the presence of the optomechanical interaction, which takes the form

$$\begin{aligned}X_{eff}^{-1}(\omega) &= \chi_m^{*-1}(-\omega)\chi_m^{-1}(\omega) - 2i|g|^2\omega_m \\ &\quad \times [\chi_c(\omega) - \chi_c^*(-\omega)].\end{aligned} \tag{A5}$$

Then the fluctuation of the cavity mode modulated by the mechanical motion can be described as

$$\begin{aligned}d(\omega) &= d_s(\omega) + d_F(\omega), \\ d_s(\omega) &= \sqrt{\kappa_{ex}}\chi_c(\omega)[1 + 2i\omega_m|g|^2 X_{eff}(\omega)\chi_c(\omega)] \\ &\quad \times \alpha_s(\omega - \Delta_s), \\ d_F(\omega) &= 2i\omega_m\sqrt{\kappa_{ex}}|\chi_c(-\omega)|^2 g^2 X_{eff}(\omega)\alpha_s^*(\omega + \Delta_s).\end{aligned} \tag{A6}$$

Equation (A6) shows that the fluctuations of the cavity field can be separated into two parts, the Stokes field $d_s(\omega)$ with center frequency Δ_s and the anti-Stokes field (FWM) $d_F(\omega)$ with center frequency $-\Delta_s$.

APPENDIX B: THE REFLECTIVE FIELDS

In terms of the input–output relation of the optical cavity, $d_r(\omega) = \sqrt{\kappa_{ex}}d(\omega) - \alpha_s(\omega - \Delta_s)$ and for a monochromatic signal laser input, $\alpha_s(\omega)$ can be expressed as a delta function $\alpha_s\delta(\omega)$, so the reflective field of the cavity can be expressed as

$$d_r(\omega) = R_s(\omega)\delta(\omega - \Delta_s) + R_F(\omega)\delta(\omega + \Delta_s). \tag{B1}$$

Considering the rotating frequency ω_p, we convert Eq. (B1) into the time domain

$$d_r(t) = R_s(\Delta_s)e^{-i\omega_s t} + R_F(-\Delta_s)e^{-i\omega_F t}, \tag{B2}$$

where $\omega_F = \omega_p - \Delta_s$, and the amplitudes of the reflected signal field $R_s(\Delta_s)$ and the conjugate field $R_F(-\Delta_s)$ take the forms

$$\begin{aligned}R_s(\Delta_s) &= \{\kappa_{ex}\chi_c(\Delta_s)[1 + 2i\omega_m|g|^2 \\ &\quad \times X_{eff}(\Delta_s)\chi_c(\Delta_s)] - 1\}\alpha_s, \\ R_F(-\Delta_s) &= 2i\omega_m\kappa_{ex}|\chi_c(-\Delta_s)|^2 g^2 X_{eff}(\Delta_s)\alpha_s^*.\end{aligned} \tag{B3}$$

The power transmission, defined as the ratio of the amplified signal and conjugate field power reflected from the system divided by the input signal power, is given by

$$\begin{aligned}M_s(\Delta_s) &= \frac{|R_s(\Delta_s)|^2}{|\alpha_s|^2}, \\ M_F(-\Delta_s) &= \frac{|R_F(-\Delta_s)|^2}{|\alpha_s|^2}.\end{aligned} \tag{B4}$$

APPENDIX C: MANIPULATION OF THE OPTICAL AMPLIFIER

The optical mode can damp the motion of the mechanical resonator, which is known as the optical damping effect. Due to the large dissipation of the cavity mode, the optomechanical system stays in the weak coupling regime [14]. The effective mechanical susceptibility $X_{eff}(\omega)$ in Eq. (A5) can be approximately written as $X_{eff}^{-1}(\omega) = \omega_{eff}^2 - \omega^2 - i\omega\Gamma_{eff}$, where $\omega_{eff} = \omega_m + \delta\omega_m$ and $\Gamma_{eff} = \Gamma_m + \Gamma_{opt}$ are the effective resonance frequency and mechanical damping rate of the mechanical resonator with

$$\begin{aligned}\delta\omega_m &= |g|^2\left[\frac{\Delta_{eff} - \omega_m}{\kappa^2/4 + (\Delta_{eff} - \omega_m)^2} + \frac{\Delta_{eff} + \omega_m}{\kappa^2/4 + (\Delta_{eff} + \omega_m)^2}\right], \\ \Gamma_{opt} &= |g|^2\left[\frac{\kappa}{\kappa^2/4 + (\Delta_{eff} + \omega_m)^2} - \frac{\kappa}{\kappa^2 4 + (\Delta_{eff} - \omega_m)^2}\right].\end{aligned} \tag{C1}$$

To derive the above equations, we have used the approximation $\omega \approx \omega_m$ and $\delta\omega_m \ll \omega_m$. In the limit of the unresolved side-band regime and a small detuning, that is,

$\kappa \gg \omega_m, \Delta_{\rm eff}$, Eq. (C1) yields

$$\delta\omega_m = g_0^2 n_c \frac{2\Delta_{\rm eff}}{\kappa^2/4 + \Delta_{\rm eff}^2},$$
$$\Gamma_{\rm opt} = -g_0^2 n_c \frac{4\Delta_{\rm eff}\kappa\omega_m}{(\kappa^2/4 + \Delta_{\rm eff}^2)^2}. \quad \text{(C2)}$$

Here, $n_c = |\alpha|^2$ represents the average photon number inside the cavity, which is directly related to the input pump power by $n_c \approx 4\kappa_{\rm ex}P_p/(\kappa^2\hbar\omega_p)$. Equation (C2) shows that we can modify the optomechanical damping rate by adjusting the detuning and input power of the pump field, which further changes the effective mechanical damping rate and enables the control of the window width of the FWM.

The maximum gain of the signal field can be achieved at resonant mechanical driving ($|\Delta_s| = \omega_{\rm eff}$) in Eq. (B4), which takes the form

$$M_{\rm max} = \frac{64|g|^4\kappa_{\rm ex}^2}{\kappa^4\Gamma_{\rm eff}^2}. \quad \text{(C3)}$$

Equation (C3) indicates that the gain of the FWM process relies on the optomechanical coupling strength g and the effective mechanical damping rate. Note that $|g|^2 = g_0^2 n_c$ and $\Gamma_{\rm eff} \approx \Gamma_{\rm opt}$, so the maximum gain in Eq. (C3) can be altered by shifting the detuning of the pump field while keeping the pump power invariant. The above results indicate that manipulation of FWM can be implemented by controlling the detuning and power of the pump field.

Figures 7 and 8 show the theoretical predictions of the manipulation of the optical amplifier, where the relevant parameters are $\kappa/2\pi = 3.5\,{\rm MHz}$, $\kappa_{\rm ex}/\kappa = 0.91$, and $g_0/2\pi = 13\,{\rm Hz}$. The window width of the FWM process as a function of the power and effective detuning of the pump field is shown in Fig. 7. By setting the pump power at 15 μW and varying the pump detuning from 60 to 620 kHz, the maximum gain and bandwidth can be controlled through the optomechanical damping effect

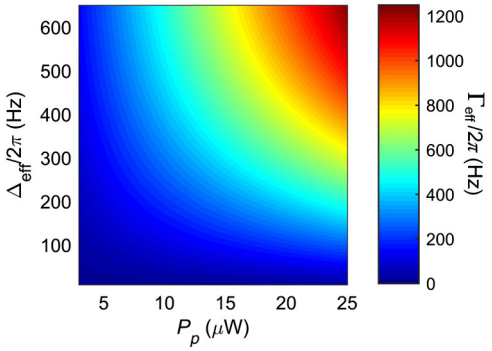

FIG. 7. Optomechanical damping rate versus the detuning and power of the pump field.

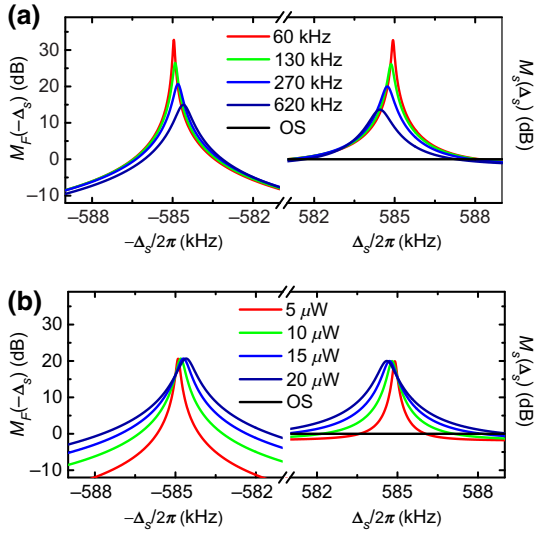

FIG. 8. Simulation of the manipulation of the optical amplifier via optomechanical FWM process by controlling the detuning (a) and input power of the pump field (b). OS, original signal. The parameters used here are the same as in Fig. 4.

[Fig. 8(a)]. The bandwidth of the amplifier can also be controlled (the maximum gain is kept almost intact) by varying the pump power while fixing the pump detuning ($\Delta_{\rm eff}/2\pi = 270\,{\rm kHz}$), as shown in Fig. 8(b).

[1] X. C. Zhao, X. P. Sun, M. H. Zhu, X. F. Wang, C. H. Ye, and X. Zhou, Atomic filter based on stimulated Raman transition at the rubidium D1 line, Opt. Express **23**, 17988 (2015).

[2] Y. Yang, X. W. Cheng, F. Q. Li, X. Hu, X. Lin, and S. S. Gong, A flat spectral faraday filter for sodium lidar, Opt. Lett. **36**, 1302 (2011).

[3] J. Hough, P. L. Bender, A. Brillet, I. Ciufolini, K. Danzmann, R. W. Hellings, A. Lobo, M. Sandford, B. F. Schutz, and P. Touboul, LISA: Laser interferometer space antenna for gravitational wave measurements, Class. Quant. Grav. **13**, 11 (1996).

[4] Jun Luo, et al., TianQin: a space-borne gravitational wave detector, Class. Quant. Grav. **33**, 035010 (2016).

[5] Paul W. McNamara, Weak-light phase-locking for LISA, Class. Quant. Grav. **22**, 243 (2005).

[6] M. W. Maeda, P. Kumar, and J. H. Shapiro, Observation of squeezed noise produced by forward four-wave mixing in sodium vapor, Opt. Lett. **12**, 161 (1987).

[7] V. Boyer, A. M. Marino, R. C. Pooser, and P. D. Lett, Entangled images from four-wave mixing, Science **321**, 544 (2008).

[8] S. K. Turitsyn, A. E. Bednyakova, M. P. Fedoruk, S. Papernyi, and W. R. L. Clements, Inverse four-wave mixing and self-parametric amplification in optical fibre, Nat. Photonics **9**, 608 (2015).

[9] T. Gu, N. Petrone, J. F. McMillan, A. van der Zande, M. Yu, G. Q. Lo, D. L. Kwong, J. Hone, and C. W. Wong,

Regenerative oscillation and four-wave mixing in graphene optoelectronics, Nat. Photonics **6**, 554 (2012).

[10] M. P. Nielsen, X. Shi, P. Dichtl, S. A. Maier, and R. F. Oulton, Giant nonlinear response at a plasmonic nanofocus drives efficient four-wave mixing, Science **358**, 1179 (2017).

[11] R. Salem, M. A. Foster, A. C. Turner, D. F. Geraghty, M. Lipson, and A. L. Gaeta, Signal regeneration using low-power four-wave mixing on silicon chip, Nat. Photonics **2**, 35 (2008).

[12] A. Gerakis, Y.-W. Yeh, M. N. Shneider, J. M. Mitrani, B. C. Stratton, and Y. Raitses, Four-Wave-Mixing Approach to in Situ Detection of Nanoparticles, Phys. Rev. Appl. **9**, 014031 (2018).

[13] V. Kravtsov, R. Ulbricht, J. M. Atkin, and M. B. Raschke, Plasmonic nanofocused four-wave mixing for femtosecond near-field imaging, Nat. Nanotechnol. **11**, 459 (2016).

[14] M. Aspelmeyer, T. J. Kippenberg, and F. Marquardt, Cavity optomechanics, Rev. Mod. Phys. **86**, 1391 (2014).

[15] Y. Ma, S. L. Danilishin, C. Zhao, H. Miao, W. Z. Korth, Y. Chen, R. L. Ward, and D. Blair, Narrowing the Filter-Cavity Bandwidth in Gravitational-Wave Detectors via Optomechanical Interaction, Phys. Rev. Lett. **113**, 151102 (2014).

[16] S. Weis, R. Riviere, S. Deleglise, E. Gavartin, Q. Arcizet, A. Schliesser, and T. J. Kippenberg, Optomechanically induced transparency, Science **330**, 1520 (2010).

[17] A. H. Safavi-Naeini, T. P. Mayer Alegre, J. Chan, M. Eichenfield, M. Winger, Q. Lin, J. T. Hill, D. E. Chang, and O. Painter, Electromagnetically induced transparency and slow light with optomechanics, Nature (London) **472**, 69 (2011).

[18] F. Massel, T. T. Heikkilä, J.-M. Pirkkalainen, S. U. Cho, H. Saloniemi, P. J. Hakonen, and M. A. Sillanpää, Microwave amplification with nanomechanical resonators, Nature (London) **480**, 351 (2011).

[19] Z. Shen, Y. L. Zhang, Y. Chen, C. L. Zou, Y. F. Xiao, X. B. Zou, F. W. Sun, G. C. Guo, and C. H. Dong, Experimental realization of optomechanically induced non-reciprocity, Nat. Photonics **10**, 657 (2016).

[20] M. Karuza, C. Biancofiore, M. Bawaj, C. Molinelli, M. Galassi, R. Natali, P. Tombesi, G. Di Giuseppe, and D. Vitali, Optomechanically induced transparency in a membrane-in-the-middle setup at room temperature, Phys. Rev. A **88**, 013804 (2013).

[21] A. Metelmann and A. A. Clerk, Quantum-Limited Amplification via Reservoir Engineering, Phys. Rev. Lett. **112**, 133904 (2014).

[22] J. P. Mathew, R. N. Patel, A. Borah, R. Vijay, and M. M. Deshmukh, Dynamical strong coupling and parametric amplification of mechanical modes of graphene drums, Nat. Nano. **11**, 747 (2016).

[23] A. Nunnenkamp, V. Sudhir, A. K. Feofanov, A. Roulet, and T. J. Kippenberg, Quantum-Limited Amplification and Parametric Instability in the Reversed Dissipation Regime of Cavity Optomechanics, Phys. Rev. Lett. **113**, 023604 (2014).

[24] W. H. P. Nielsen, Y. Tsaturyan, C. B. Moller, E. S. Polzik, and A. Schliesser, Multimode optomechanical system in the quantum regime, Proc. Nat. Acad. Sci. U. S. A **114**, 62 (2017).

[25] A. H. Safavi-Naeini, S. Gröblacher, J. T. Hill, J. Chan, M. Aspelmeyer, and O. Painter, Squeezed light from a silicon micromechanical resonator, Nature (London) **500**, 185 (2013).

[26] E. E. Wollman, C. U. Lei, A. J. Weinstein, J. Suh, A. Kronwald, F. Marquardt, A. A. Clerk, and K. C. Schwab, Quantum squeezing of motion in a mechanical resonator, Science **349**, 952 (2015).

[27] S. Barzanjeh, E. S. Redchenko, M. Peruzzo, M. Wulf, D. P. Lewis, G. Arnold, and J. M. Fink, Stationary entangled radiation from micromechanical motion, arXiv:1809.05865 (2019).

[28] Y. Wang, S. Chesi, and A. A. Clerk, Bipartite and tripartite output entanglement in three-mode optomechanical systems, Phys. Rev. A **91**, 013807 (2015).

[29] X. You, and Y. M. Li, Strong quantum entanglement via a controllable four wave mixing mechanism in an optomechanical system, arXiv:1905.07978 (2019).

[30] R. W. Andrews, R. W. Peterson, T. P. Purdy, K. Cicak, R. W. Simmonds, C. A. Regal, and K. W. Lehnert, Bidirectional and efficient conversion between microwave and optical light, Nat. Phys. **10**, 321 (2014).

[31] S.-M. Huang and G. Agarwal, Normal-mode splitting and antibunching in Stokes and anti-Stokes processes in cavity optomechanics: Radiation-pressure-induced four-wave-mixing cavity optomechanics, Phys. Rev. A **81**, 033830 (2010).

[32] W. Z. Jia, L. F. Wei, Y. Li, and Y.-X. Liu, Phase-dependent optical response properties in an optomechanical system by coherently driving the mechanical resonator, Phys. Rev. A **91**, 043843 (2015).

[33] J. Ma, C. You, L. G. Si, H. Xiong, J. H. Li, X. Yang, and Y. Wu, Optomechanically induced transparency in the presence of an external time-harmonic-driving force, Sci. Rep. **5**, 11278 (2015).

[34] Z. Y. Li, X. You, Y. M. Li, Y.-C. Liu, and K. C. Peng, Multimode four-wave mixing in an unresolved sideband optomechanical system, Phys. Rev. A **97**, 033806 (2018).

[35] T. Kessler, C. Hagemann, C. Grebing, T. Legero, U. Sterr, F. Riehle, M. J. Martin, L. Chen, and J. Ye, A sub-40-mHz-linewidth laser based on a silicon single-crystal optical cavity, Nat. Photonics **6**, 687 (2012).

[36] J. D. Thompson, B. M. Zwickl, A. M. Jayich, F. Marquardt, S. M. Girvin, and J. G. E. Harris, Strong dispersive coupling of a high-finesse cavity to a micromechanical membrane, Nature (London) **452**, 72 (2008).

[37] D. J. Wilson, C. A. Regal, S. B. Papp, and H. J. Kimble, Cavity Optomechanics with Stoichiometric SiN Films, Phys. Rev. Lett. **103**, 207204 (2009).

[38] M. Rossi, N. Kralj, S. Zippilli, R. Natali, A. Borrielli, G. Pandraud, E. Serra, G. Di Giuseppe, and D. Vitali, Normal-Mode Splitting in a Weakly Coupled Optomechanical System, Phys. Rev. Lett. **120**, 073601 (2018).

[39] T. P. Purdy, R. W. Peterson, and C. A. Regal, Observation of radiation pressure shot noise on a macroscopic object, Science **339**, 801 (2013).